Supporting Information

Few-layered $Ti_3C_2T_x$ MXene coupled with Fe_2O_3 nanorod arrays grown on carbon cloth as anodes for flexible asymmetric supercapacitors

Fei Li[1,†], Yi-Lin Liu[1,†], Gui-Gen Wang[*,†], Hua-Yu Zhang[†], Bin Zhang[†],

Gui-Zhong Li[†], Zhi-Peng Wu[†], Le-Yang Dang[†], Jie-Cai Han[†,‡]

[†]*Shenzhen Key Laboratory for Advanced Materials, Harbin Institute of Technology, Shenzhen, Shenzhen 518055, China*

[‡]*Center for Composite Materials, Harbin Institute of Technology, Harbin 150080, China*

Corresponding author (G.G. Wang). Tel: +86-755-26629471, fax: +86-755-26033504.

E-mail: wangguigen@hit.edu.cn

Table S1.The mass of Mxene coated on Fe_2O_3/CC varied with dipping times (the Fe_2O_3 loading mass on CC was about 1.35 mg cm^{-2})

Mxene@Fe_2O_3/CC composite	0.5-Mxene@ Fe_2O_3/CC	1-Mxene@ Fe_2O_3/CC	1.5-Mxene@ Fe_2O_3/CC	2-Mxene@ Fe_2O_3/CC
Dipping times	4	7	9	12
Loading mass of Mxene (mg cm^{-2})	0.53	1.04	1.48	2.02

As to the 1.0-Mxene@Fe_2O_3/CC, 1.5-Mxene@Fe_2O_3/CC, and 2.0-Mxene@Fe_2O_3/CC electrode, the Mxene sheets almost coated the Fe_2O_3/CC completely. With the increase content of Mxene in the composites, the increasing value of specific capacitance is almost equal. The specific capacitance of 1.0-Mxene@Fe_2O_3/CC (1), 1.5-Mxene@Fe_2O_3/CC (2), and 2.0-Mxene@Fe_2O_3/CC (3) is 446, 579, and 725 mF cm^{-2}, respectively. The area capacitance of (2)-(1) is approximately equal to that of (3)-(2) which is about 140 mF cm^{-2}, suggesting that the increased capacitance was attributed by added Mxene when the Fe_2O_3/CC was coated completely by the Mxene sheets. In addition, as shown from the SEM images in Fig. S7, it can be observed that the Fe_2O_3/CC was coated gradually with the increase of Mxene content. Among the 2.0-Mxene@Fe_2O_3/CC flexible electrode, the Fe_2O_3/CC was completely wrapped by the Mxene sheet compared with the other three electrodes. Therefore, based on above these results, the 2.0-Mxene@Fe_2O_3/CC is considered as the desired loading mass.

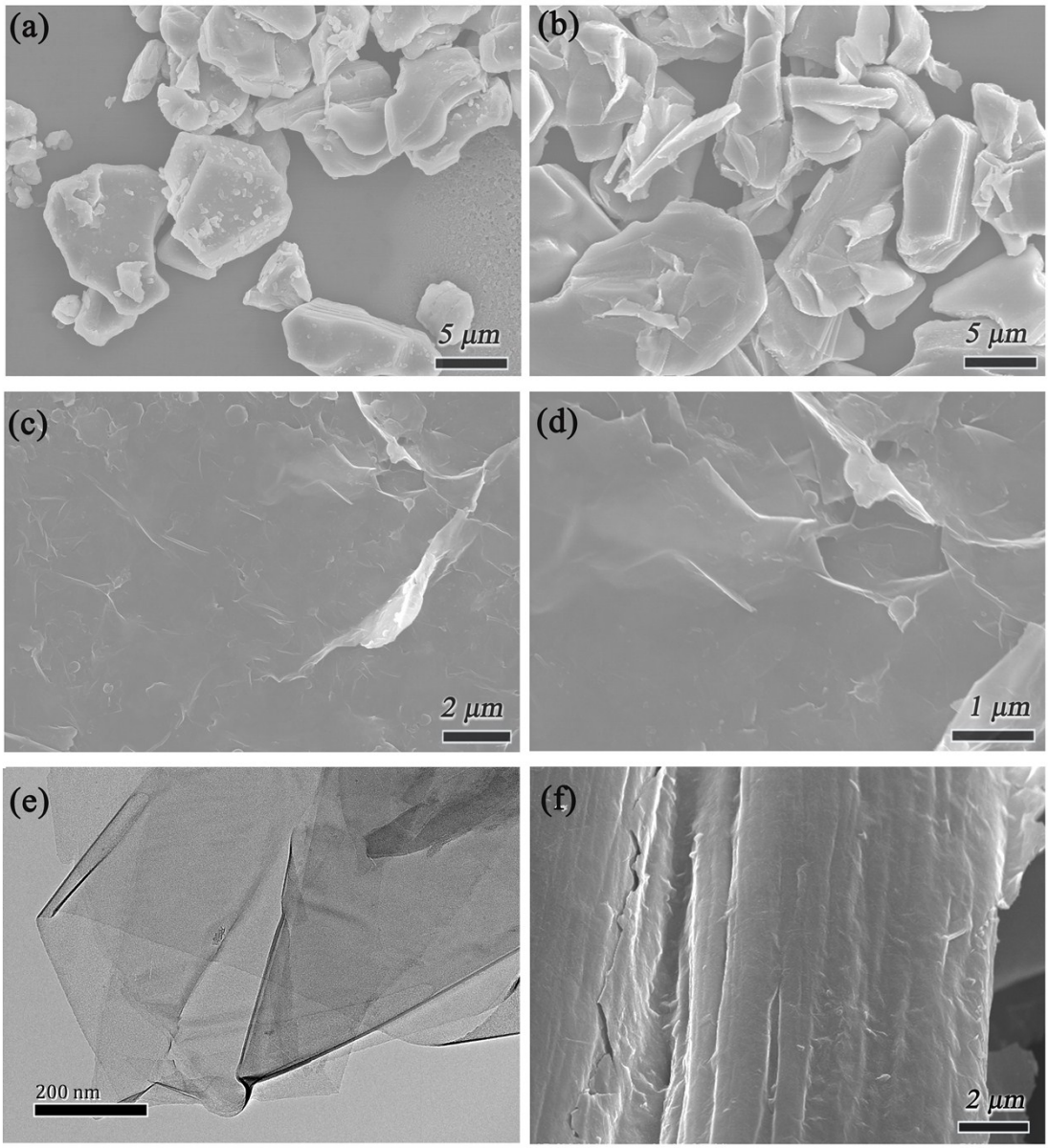

Fig. S1 SEM images of (a) the pristine Max(Ti_3AlC_2) and (b) the non-delaminated Ti_2CT_x Mxene which is the sediment centrifuged at 1000 rpm for 5 min. (c,d) SEM images of Mxene sheets with different magnifications, (e) TEM image of Mxene sheets, (f) Surface SEM image of Mxene/CC.

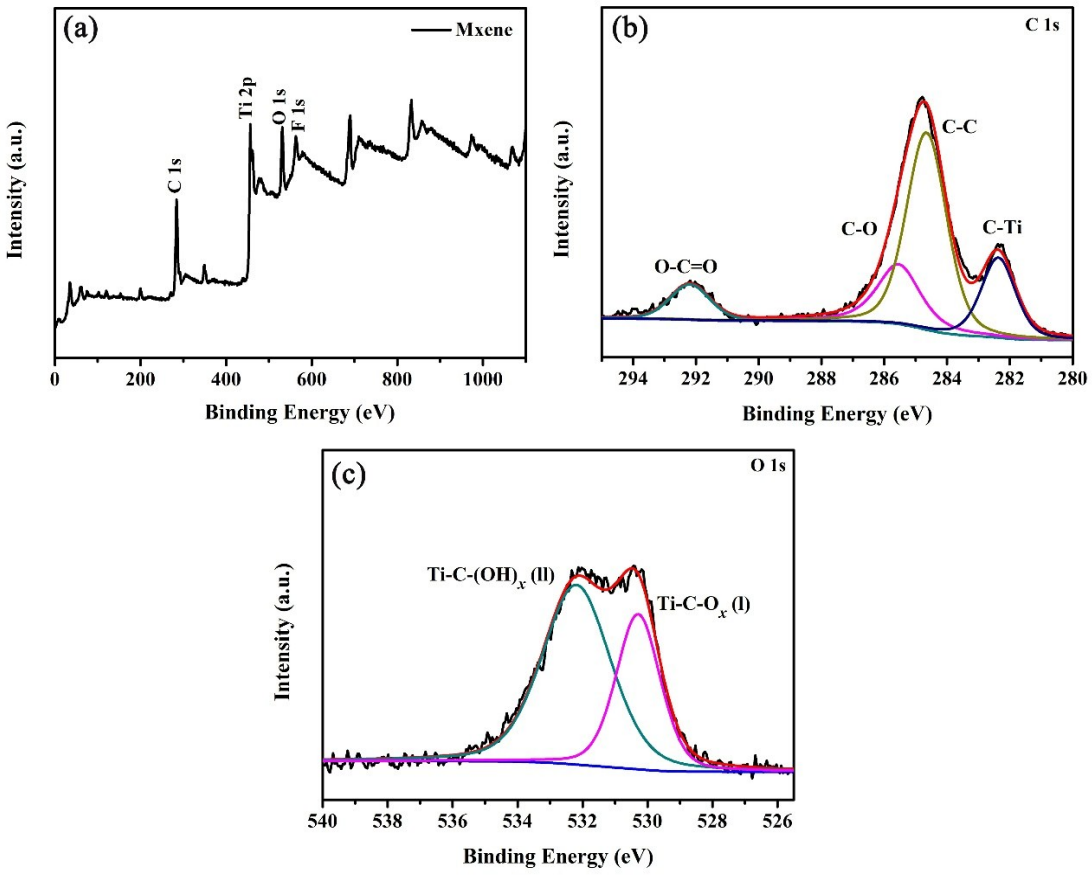

Fig. S2 (a) XPS survey spectrum of the delaminated Ti_2CT_x Mxene.
(b-c) High-resolution XPS spectra of C 1s and O 1s.

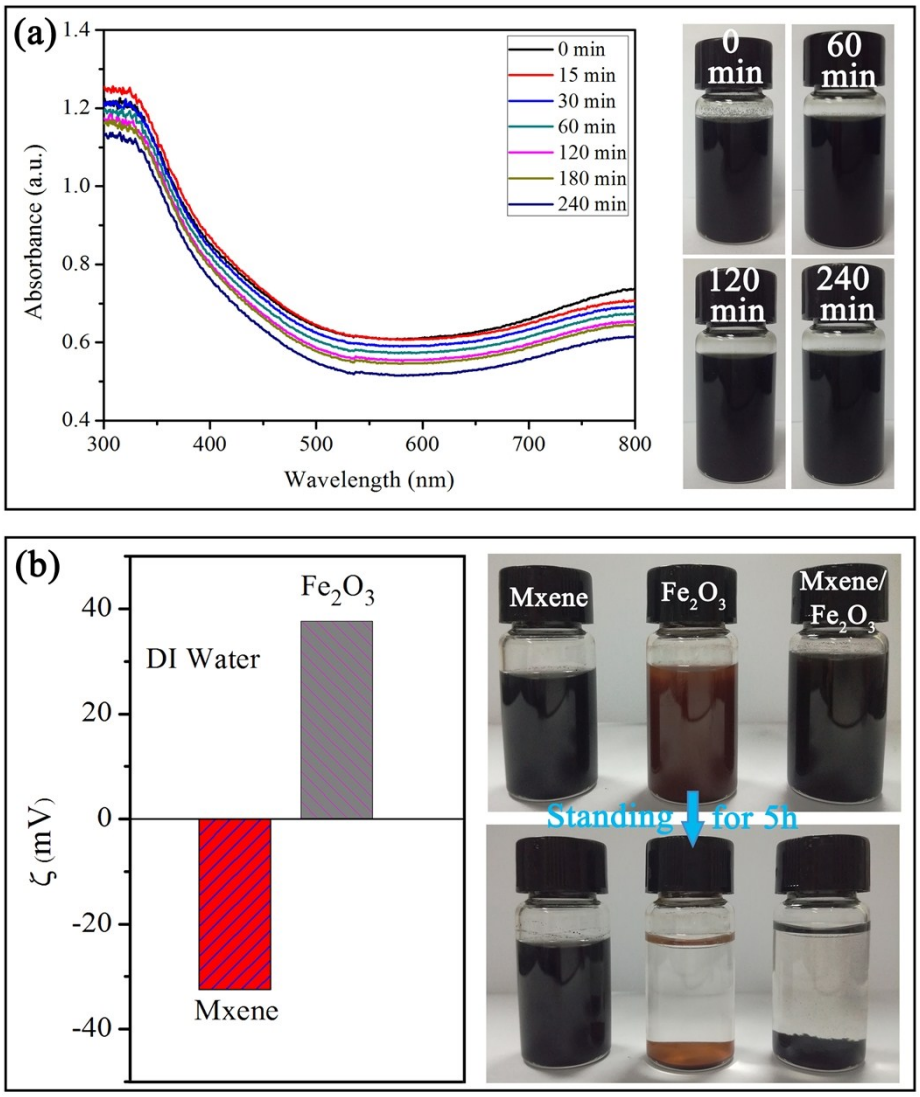

Fig. S3 (a) The UV-Vis spectra and digital photographs of Mxene solution after different standing time. The Mxene solution (1mg/mL) was standing for different time, then 0.5 mL of Mxene solution was taken out and diluted for 20 times. (b) Zeta potentials of Mxene and Fe_2O_3 in DI water, and the digital photographs of Mxene, Fe_2O_3, and Mxene/ Fe_2O_3 solution for standing 5 hours.

The Mxene sheets contain many termination functional groups (-O, -OH, and -F), benefiting for metallic oxides to bond together by electrostatic interaction. The ζ values of Mxene and Fe_2O_3 in DI water are -32.5 and 37.7 mV, respectively. The opposite potentials of Mxene and Fe_2O_3 can contribute to their attraction each other. In addition, the Mxene solution remains good dispersion, and the mixed solutions of Fe_2O_3 and Mxene/Fe_2O_3 was completely deposited at the bottom of sample bottles after standing for 5 hours. The Mxene sheet was completely subsided along with Fe_2O_3, which

indicates that the Mxene sheet and Fe_2O_3 exist strong interaction to result in their depositing together. Therefore, the Mxene sheet can adhere to the Fe_2O_3/CC fibres and form coating on its surface gradually when the Fe_2O_3/CC dips into the Mxene solution. In addition, the 2D Mxene sheets tend to self-assemble layer-by-layer and the wrapped shells are formed on the surfaces of Fe_2O_3/CC fibres.

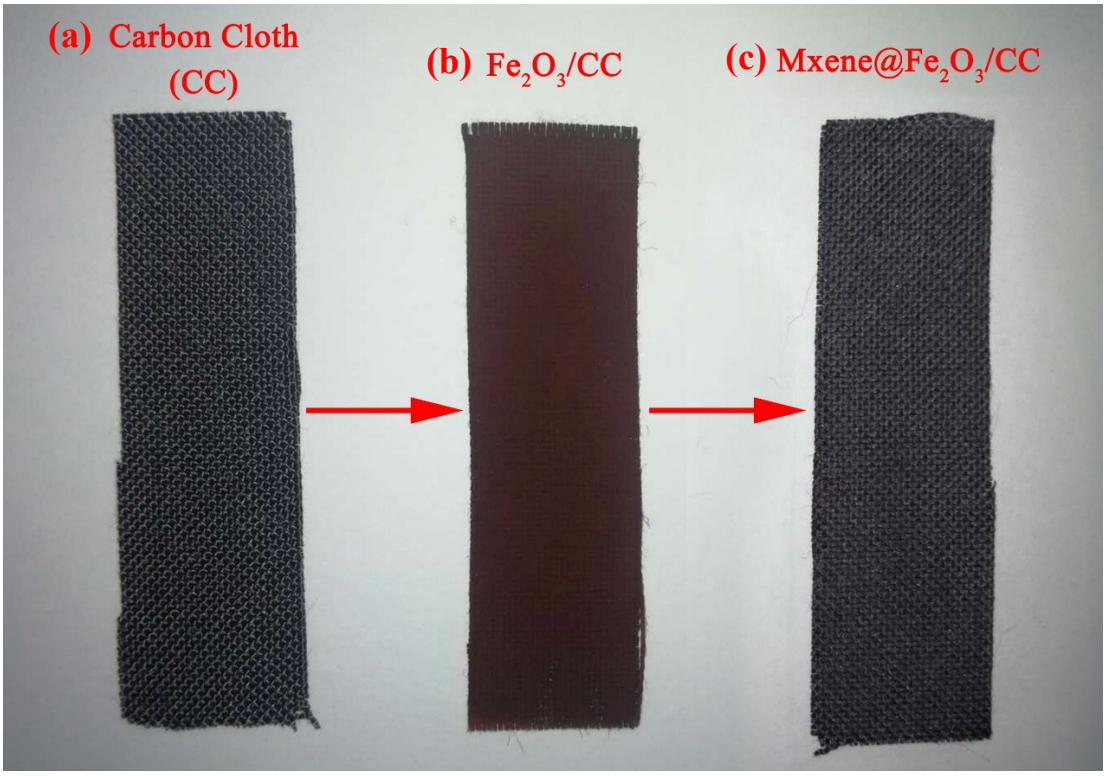

Fig. S4 The digital photographs of pristine CC (a), Fe_2O_3/CC (b), and Mxene@ Fe_2O_3/CC (c).

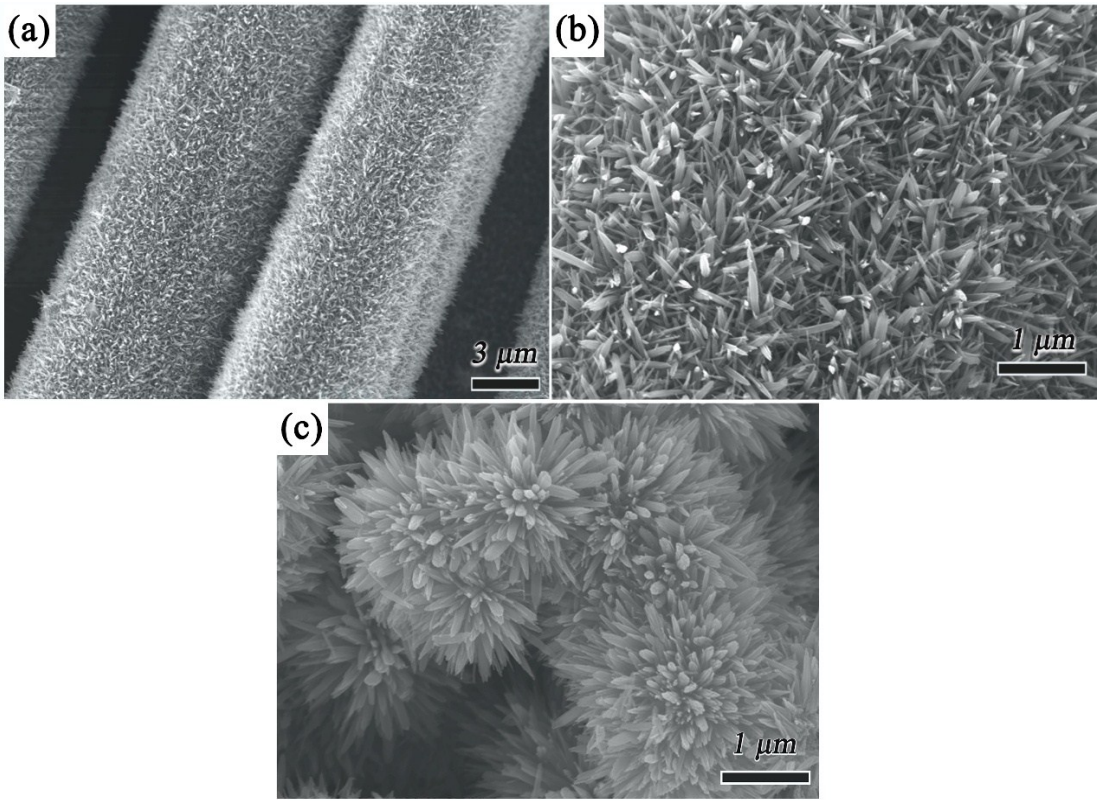

Fig. S5 SEM images of (a) the Fe_2O_3/CC in which the Fe_2O_3 was uniformly grown on each carbon fibre, (b) high-magnification image of Fe_2O_3 which looks like the grass, and (c) the powder of Fe_2O_3 with an urchin-like shape.

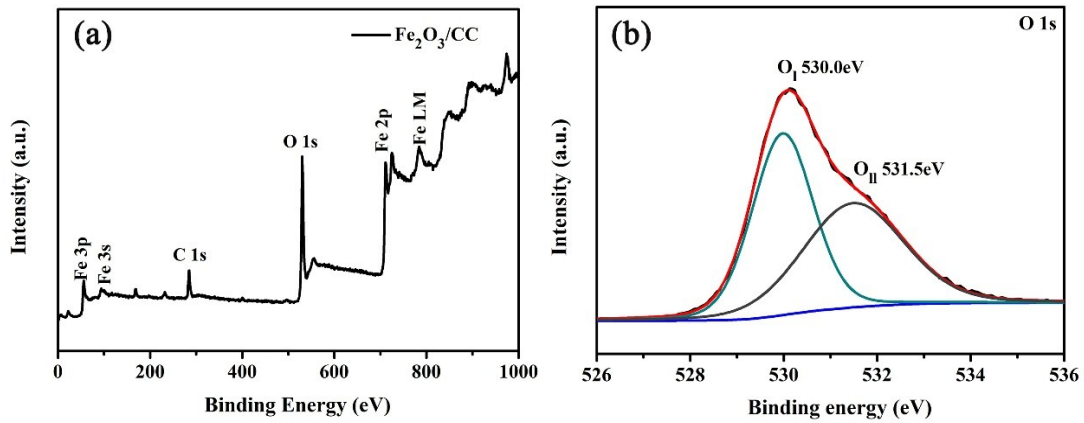

Fig. S6 (a) XPS survey spectrum of the Fe_2O_3/CC. (b) High-resolution XPS spectrum of O 1s.

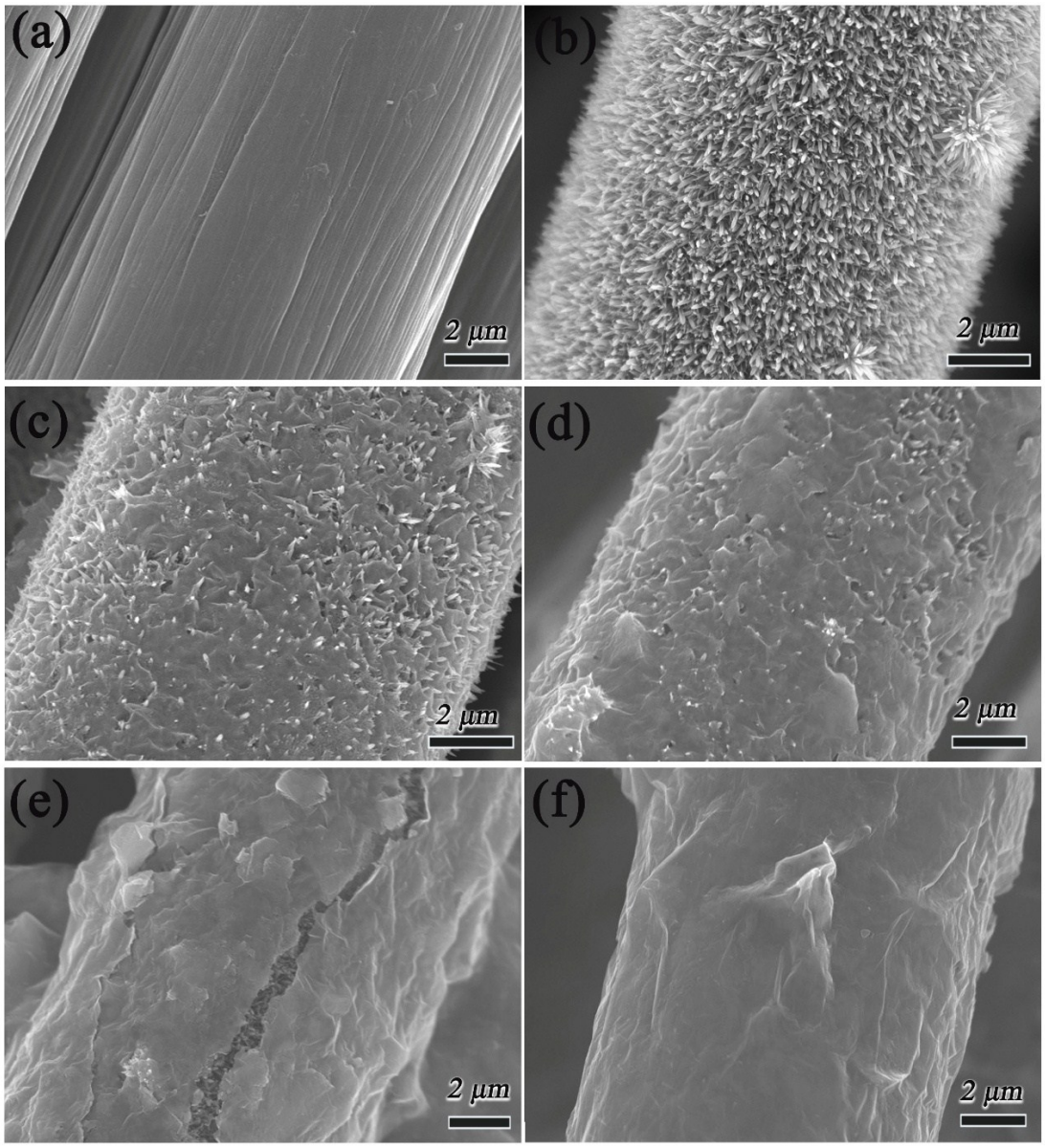

Fig. S7 SEM images of the pristine carbon fiber (a), Fe_2O_3/CC (b), and Mxene@Fe_2O_3/CC with different loading contents of Mxene (c-f). The Fe_2O_3/CC was gradually coated by Mxene with the increase of dipping time in Mxene solution.

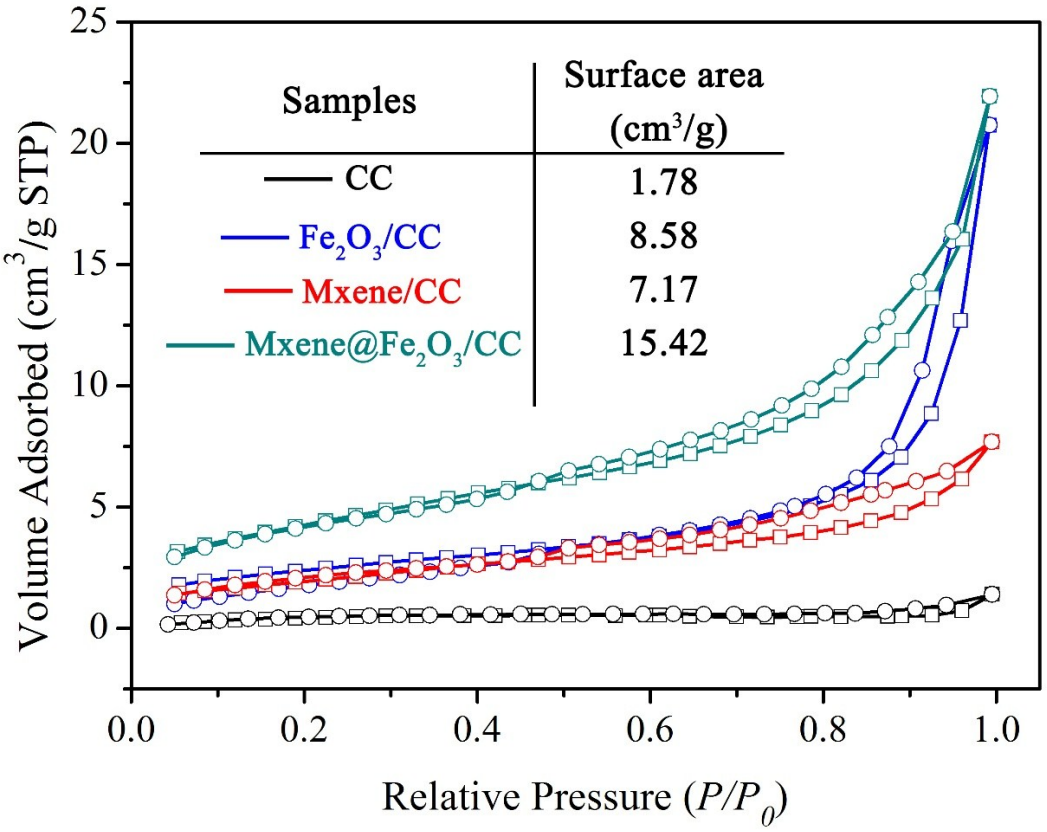

Fig. S8 N_2 adsorption-desorption isotherm of the carbon cloth (CC) and Fe_2O_3/CC, Mxene/CC, and Mxene@Fe_2O_3/CC.

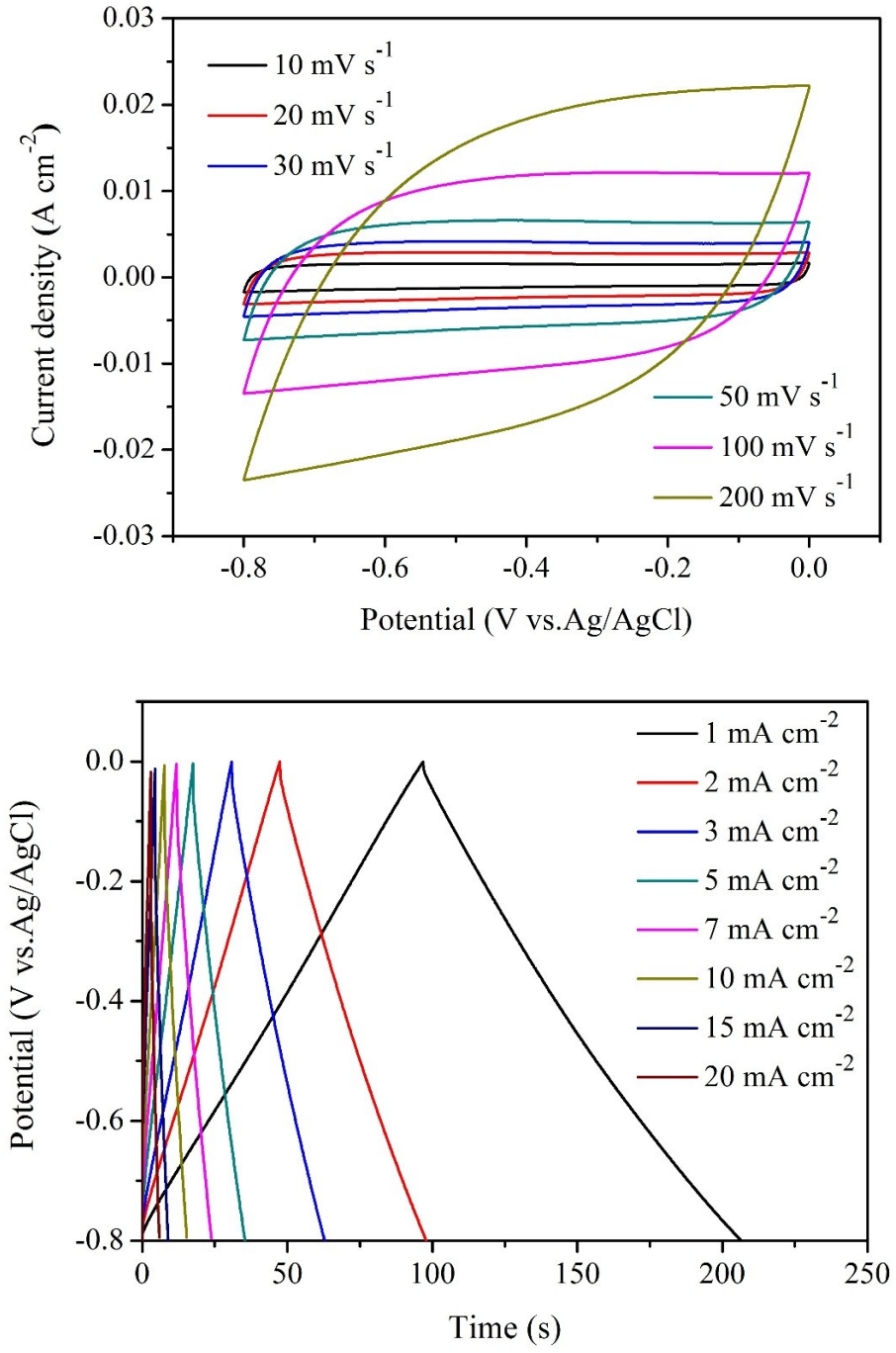

Fig. S9 (a) CV curves of the Mxene/CC electrodes at different scan rates. (b) GCD curves of the Mxene/CC electrodes at different current densities.

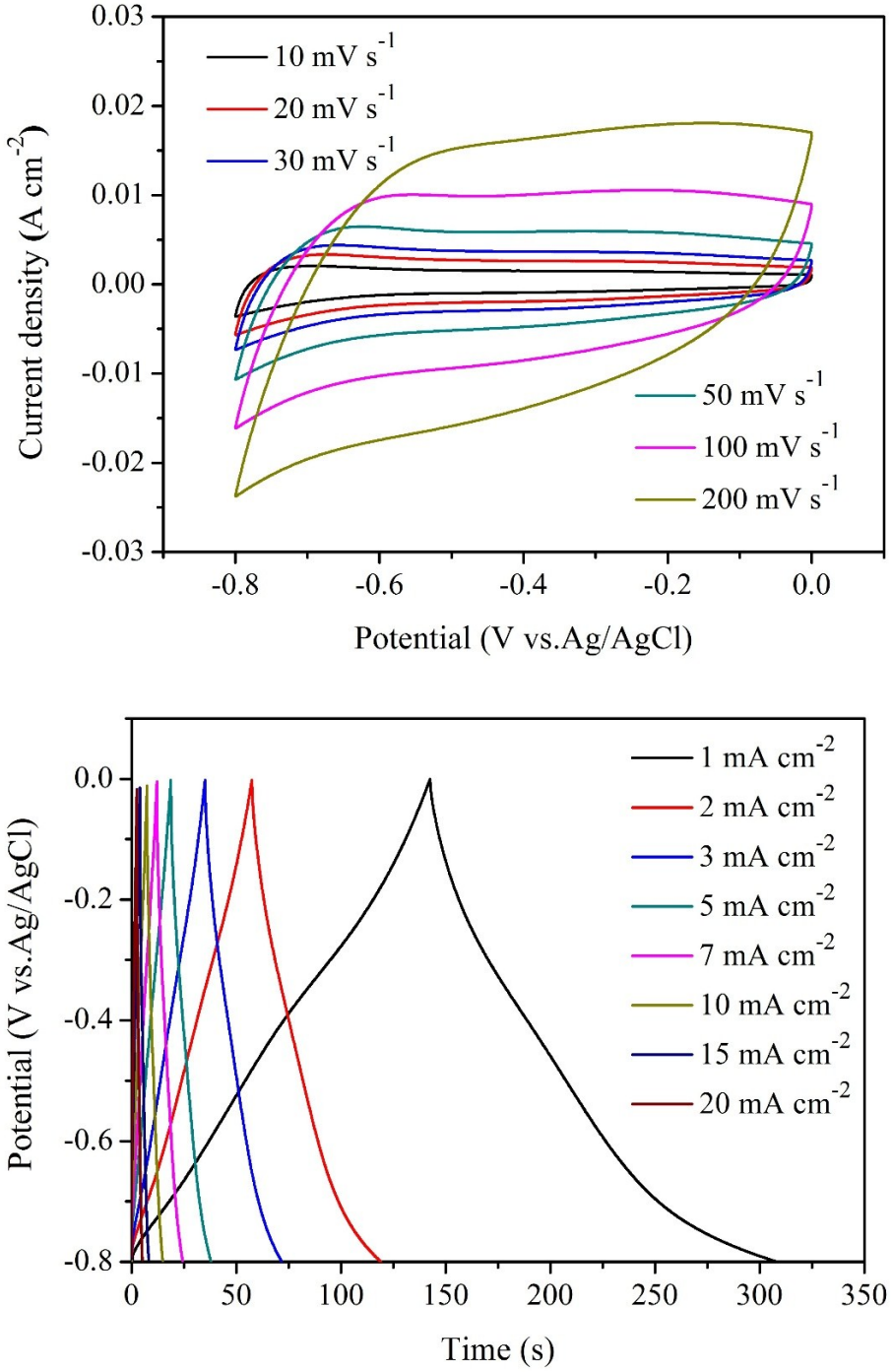

Fig. S10 (a) CV curves of the Fe_2O_3/CC electrodes at different scan rates. (b) GCD curves of the Fe_2O_3/CC electrodes at different current densities.

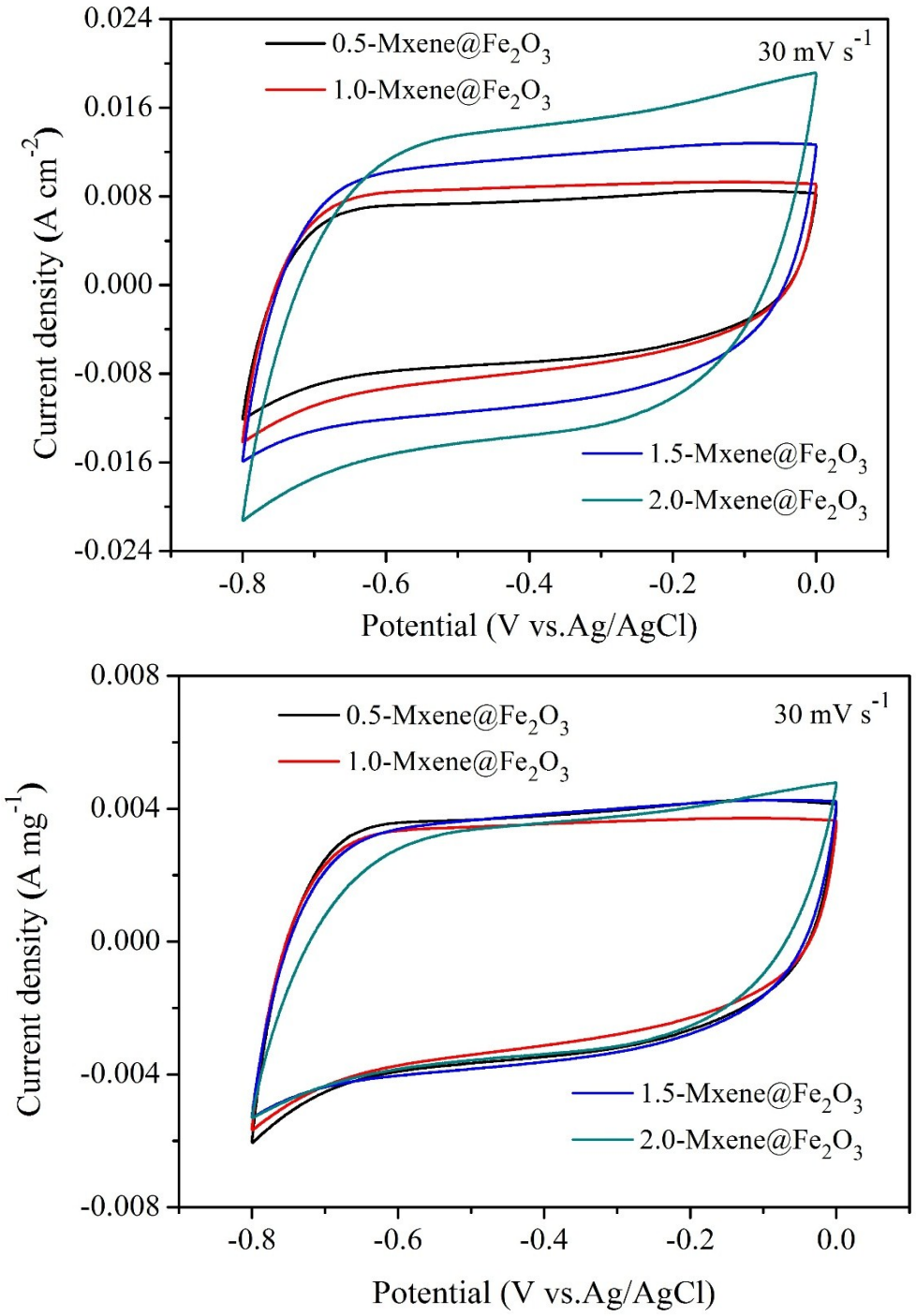

Fig. S11 CV curves of Mxene@Fe_2O_3/CC with different loading masses of Mxene at 30 mV/s. Normalized by (a) electrode area (cm^2) and (b) mass of the active material of electrode (mg).

Table S2. Comparison of Fe_2O_3 anodes for supercapacitors.

Electrode	Electrolyte	Capacitance	Current density	Reference
N-C/Fe_2O_3	5 M LiCl	148.5 mF cm^{-2}	0.5 mA cm^{-2}	[1]
Fe_2O_3@C NRAs	1 M KOH	194 mF cm^{-2}	2 mA cm^{-2}	[2]
T-Fe_2O_3/Ppy	1 M Na_2SO_4	382.4 mF cm^{-2}	0.5 mA cm^{-2}	[3]
crystalline/amorphous $Fe_2O_{3-\delta}$	1 M LiOH	350 mF cm^{-2}	1 mA cm^{-2}	[4]
Oxygen-deficient Fe_2O_3 nanorods	5 M LiCl	382.7 mF cm^{-2}	0.5 mA cm^{-2}	[5]
Fe_2O_3 NTs	5 M LiCl	180.4 mF cm^{-2}	1 mA cm^{-2}	[6]
Fe_2O_3-P nanorods	1 M Na_2SO_4	340 mF cm^{-2}	1 mA cm^{-2}	[7]
α-Fe_2O_3/C nanoarrays	1 M Na_2SO_4	430.8 mF cm^{-2}	1 mA cm^{-2}	[8]
α-Fe_2O_3@PANI	1 M Na_2SO_4	103 mF cm^{-2}	0.86 mA cm^{-2}	[9]
a-Fe_2O_3@NiO	1 M LiOH	557 mF cm^{-2}	1 mA cm^{-2}	[10]
Ni/GF/H-Fe_2O_3	3 M KOH	694 mF cm^{-2}	1 mA cm^{-2}	[11]
Mxene@Fe_2O_3/CC	5 M LiCl	725 mF cm^{-2}	1 mA cm^{-2}	This work

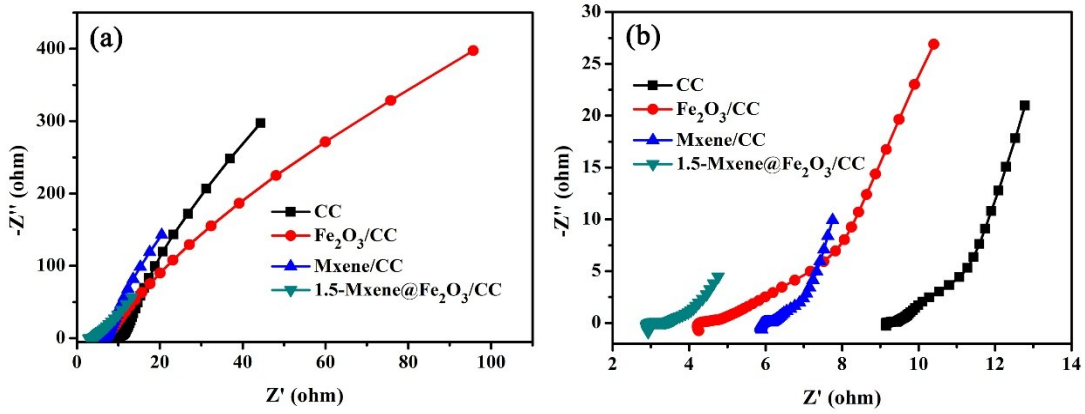

Fig. S12 Nyquist plots of CC, Fe_2O_3/CC, Mxene /CC, 1.5-Mxene@Fe_2O_3/CC electrodes (a) and the enlarged at high frequency (b). The Mxene and CC possess excellent conductivity and there are less interfacial charge transfers between these, so the ESR of MXene/CC is much larger than that of Fe_2O_3/CC electrode at high-frequency range.

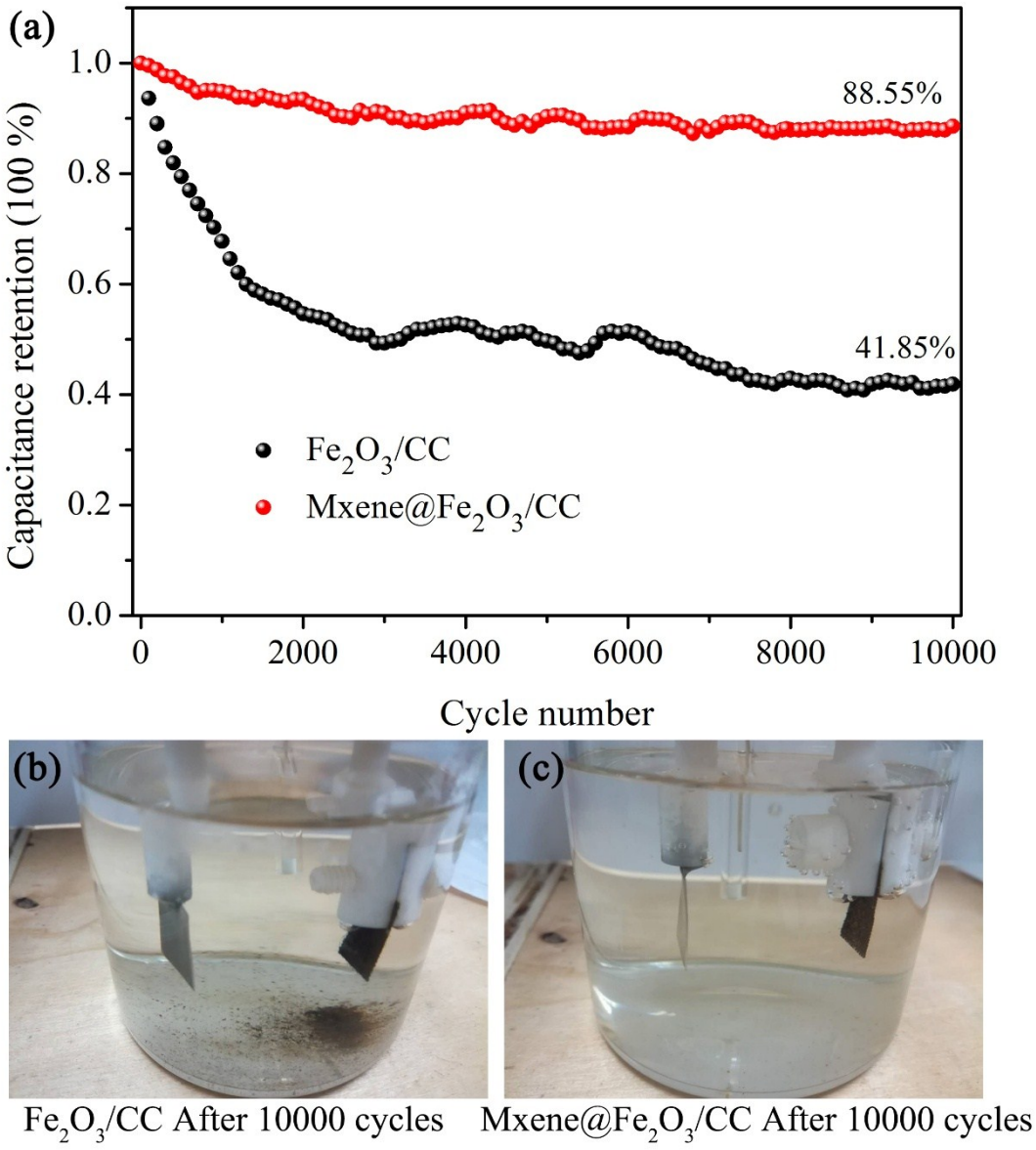

Fig. S13 (a) Cycling performances of the Fe_2O_3/CC, Mxene@Fe_2O_3/CC electrodes for 10000 cycles and the digital photographs of (b) Fe_2O_3/CC, (c) Mxene@Fe_2O_3/CC after 10000 cycles.

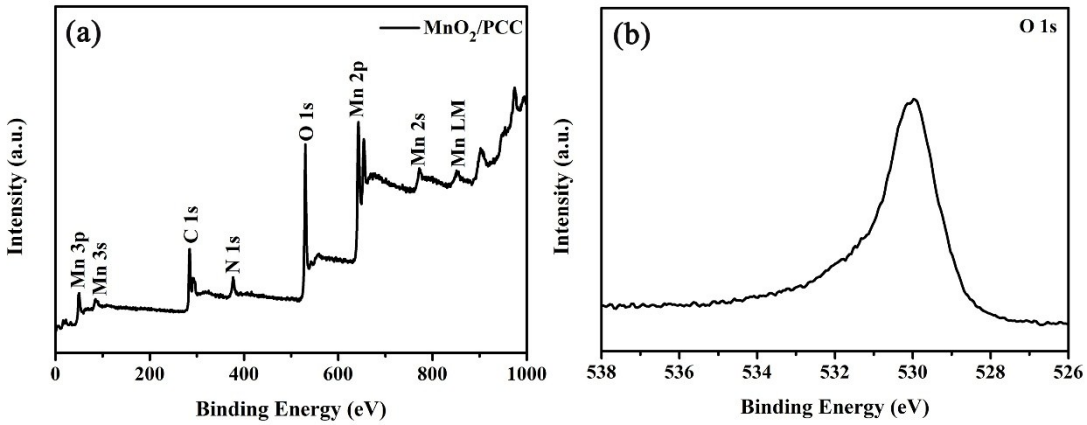

Fig. S14 (a) XPS survey spectrum of the MnO_2/PCC. (b) High-resolution XPS spectrum of O 1s.

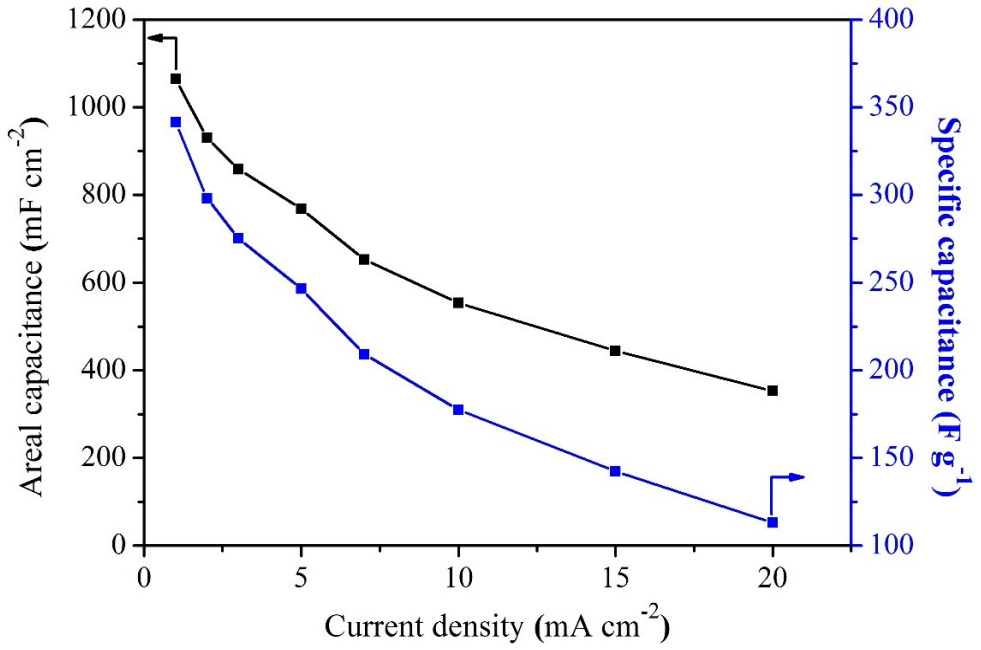

Fig. S15 Areal (mF cm^{-2}) and specific (F g^{-1}) capacitance of MnO_2/PCC electrode at different current densities.

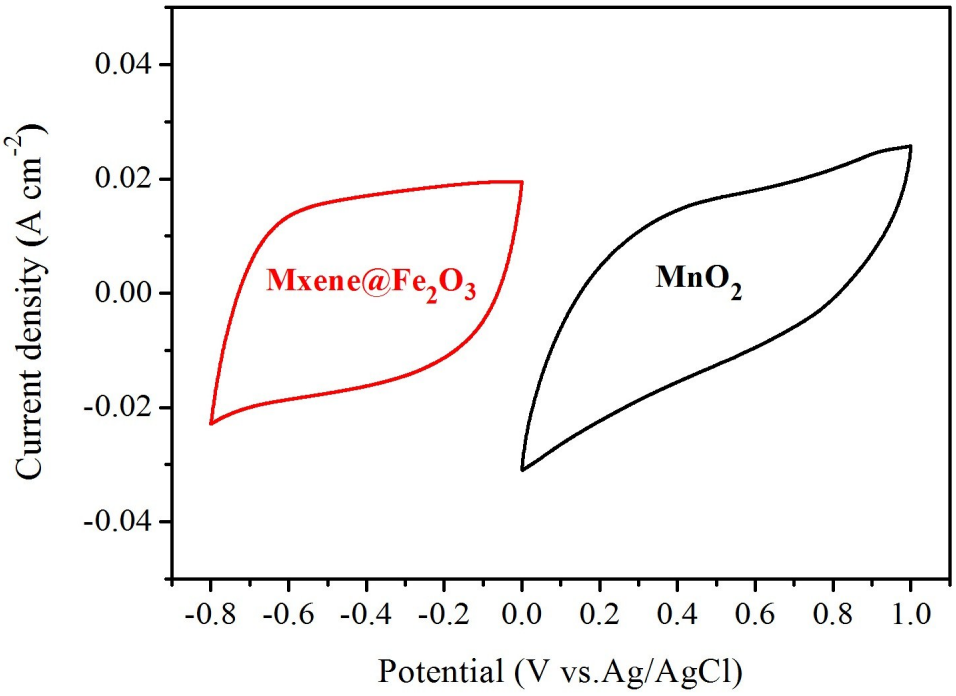

Fig. S16 CV curves collected for MnO_2/PCC and Mxene@Fe_2O_3/CC electrodes at a scan rate of 50 mV s^{-1}

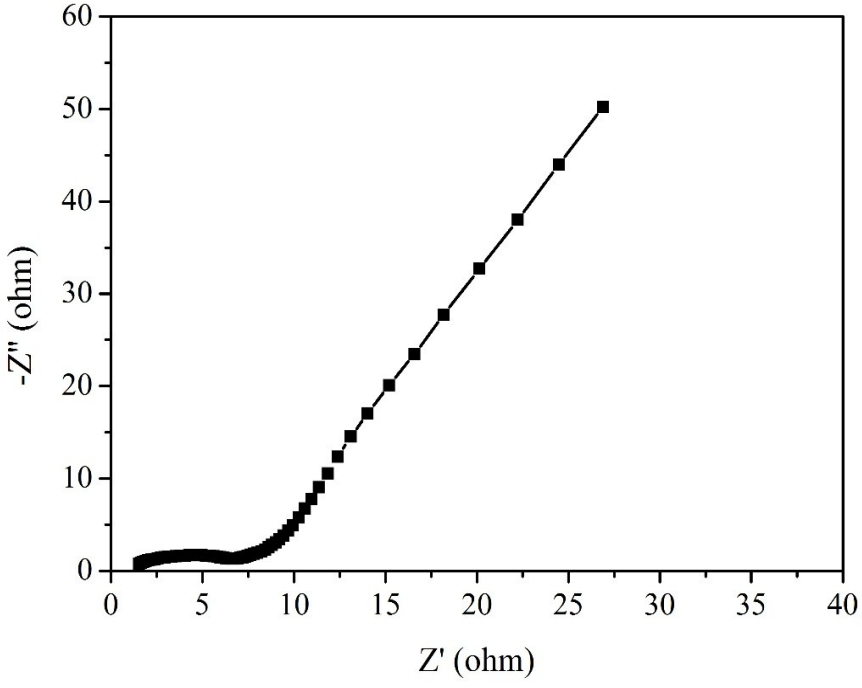

Fig. S17 EIS of the as-assembled MnO_2/PCC// Mxene@Fe_2O_3/CC ASCs

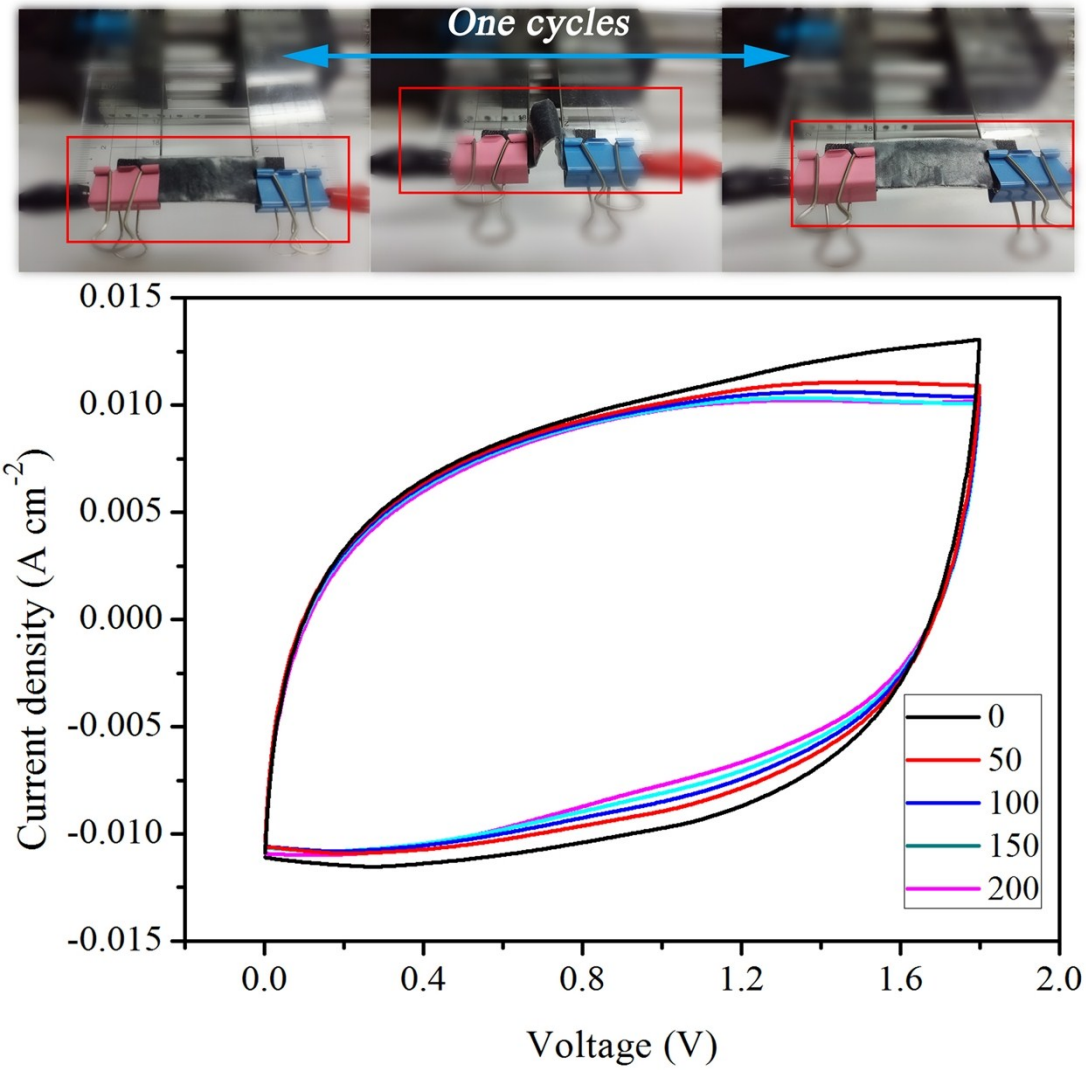

Fig. S18 CV curves of the MnO_2/PCC//Mxene@Fe_2O_3/CC-ASC device collected at a scan rate of 100 mV s^{-1}, the device were bended and then released after 50, 100, 150, and 200 times, in which there were digital photographs during one cycle.

Reference:

[1] Fu W, Zhao E, Ren X, et al. Hierarchical fabric decorated with carbon nanowire/metal oxide nanocomposites for 1.6 V wearable aqueous supercapacitors[J]. Advanced Energy Materials, 2018, 8(18): 1703454.

[2] Yang Q, Li Z, Zhang R, et al. Carbon modified transition metal oxides/hydroxides nanoarrays toward high-performance flexible all-solid-state supercapacitors[J]. Nano Energy, 2017, 41: 408-416.

[3] Wang L, Yang H, Liu X, et al. Constructing Hierarchical Tectorum-like α-Fe_2O_3/PPy Nanoarrays on Carbon Cloth for Solid-State Asymmetric Supercapacitors[J]. Angewandte Chemie International Edition, 2017, 56(4): 1105-1110.

[4] Sun S, Zhai T, Liang C, et al. Boosted crystalline/amorphous $Fe_2O_{3-\delta}$ core/shell heterostructure for flexible solid-state pseudocapacitors in large scale[J]. Nano Energy, 2018, 45: 390-397.

[5] Lu X, Zeng Y, Yu M, et al. Oxygen-deficient hematite nanorods as high-performance and novel negative electrodes for flexible asymmetric supercapacitors[J]. Advanced materials, 2014, 26(19): 3148-3155.

[6] Yang P, Ding Y, Lin Z, et al. Low-cost high-performance solid-state asymmetric supercapacitors based on MnO_2 nanowires and Fe_2O_3 nanotubes[J]. Nano letters, 2014, 14(2): 731-736.

[7] Liang H, Xia C, Emwas A H, et al. Phosphine plasma activation of α-Fe_2O_3 for high energy asymmetric supercapacitors[J]. Nano energy, 2018, 49: 155-162.

[8] Chen D, Zhou S, Quan H, et al. Tetsubo-like α-Fe_2O_3/C nanoarrays on carbon cloth as negative electrode for high-performance asymmetric supercapacitors[J]. Chemical Engineering Journal, 2018, 341: 102-111.

[9] Lu X F, Chen X Y, Zhou W, et al. α-Fe_2O_3@PANI core-shell nanowire arrays as negative electrodes for asymmetric supercapacitors[J]. ACS applied materials & interfaces, 2015, 7(27): 14843-14850.

[10] Jiao Y, Liu Y, Yin B, et al. Hybrid α-Fe_2O_3@NiO heterostructures for flexible and high performance supercapacitor electrodes and visible light driven photocatalysts[J]. Nano Energy, 2014, 10: 90-98.

[11] Chi K, Zhang Z, Lv Q, et al. Well-ordered oxygen-deficient $CoMoO_4$ and Fe_2O_3 nanoplate arrays on 3D graphene foam: toward flexible asymmetric supercapacitors with enhanced capacitive properties[J]. ACS applied materials & interfaces, 2017, 9(7): 6044-6053.